

Article

Reversible Water Ad-/Desorption Behavior of a 3D Polycatenation Network, [Zn(bpp)(BDC)]·1.5(H₂O), Constructed by 2D Undulated Layered MOF

Chih-Chieh Wang ^{1,*}, Wei-Cheng Yi ¹, Zi-Ling Huang ¹, Wen-Chi Chien ¹, Yu-Chun Chuang ^{2,*}
and Gene-Hsiang Lee ³

¹ Department of Chemistry, Soochow University, Taipei 11106, Taiwan; 06333004@gm.scu.edu.tw (W.-C.Y.); wendyhung51@gmail.com (Z.-L.H.); momo2013124@gmail.com (W.-C.C.)

² Instrumentation Center, National Taiwan University, Taipei 10617, Taiwan

³ National Synchrotron Radiation Research Center, Hsinchu 30076, Taiwan; ghlee@ntu.edu.tw

* Correspondence: ccwang@scu.edu.tw (C.-C.W.); chuang.yc@nsrrc.org.tw (Y.-C.C.);

Tel.: +886-2-28819471 (ext. 6828) (C.-C.W.)

Abstract: A three-dimensional (3D) polycatenation supramolecular network with chemical formulas, [Zn(bpp)(BDC)]·1.5H₂O (**1**), (bpp = 1,3-bis(4-pyridyl)propane, BDC²⁻ = dianion of terephthalic acid), was synthesized and structurally determined. In compound **1**, the coordination geometry of Zn(II) ion is distorted tetrahedral, where its 2D undulated layered framework is constructed via the bridges of Zn(II) ions with bpp and BDC²⁻ ligands. Adjacent 2D layers are arranged in a combined parallel and interpenetrated manner to complete its 3D polycatenation supramolecular architecture. Compound **1** shows a one-step dehydration process with the weight losses of 6.1%, approximately equal to the weight percentage of losing 1.5 guest water molecules. The cyclic thermogravimetric analysis reveals that compound **1** shows reversible, sponge-like water de-/adsorption behavior during de-/rehydration processes. Compound **1** also exhibits significant water vapor hysteresis isotherm.

Keywords: supramolecular compound; metal–organic framework; H bonding interaction; π - π stacking interaction



Citation: Wang, C.-C.; Yi, W.-C.; Huang, Z.-L.; Chien, W.-C.; Chuang, Y.-C.; Lee, G.-H. Reversible Water Ad-/Desorption Behavior of a 3D Polycatenation Network, [Zn(bpp)(BDC)]·1.5(H₂O), Constructed by 2D Undulated Layered MOF. *Crystals* **2021**, *11*, 371. <https://doi.org/10.3390/cryst11040371>

Academic Editors: Luisa De Marco and Stefano Brenna

Received: 1 February 2021

Accepted: 30 March 2021

Published: 2 April 2021

Publisher's Note: MDPI stays neutral with regard to jurisdictional claims in published maps and institutional affiliations.



Copyright: © 2021 by the authors. Licensee MDPI, Basel, Switzerland. This article is an open access article distributed under the terms and conditions of the Creative Commons Attribution (CC BY) license (<https://creativecommons.org/licenses/by/4.0/>).

1. Introduction

Crystal engineering of three-dimensional (3D) supramolecular frameworks assembled by coordination polymers (CPs) [1] or metal–organic frameworks (MOFs) with various types of structural topologies [1,2] have been widely studied not only for the structural diversity of their supramolecular chemistry but also for their potential applications [3–12]. In the field of supramolecular chemistry, entangled composites in 3D supramolecular networks constitute an important topic via the assembly of various CPs, as found in interpenetration, polycatenane, interdigitation, polythread, and other species [13–18]. CPs with different orientations entangled together within the crystals were found in the formation of fascinating 3D supramolecular networks with interpenetrated or catenated manners [19–25]. The 1,3-bis(4-pyridyl)propane (bpp), a flexible bi-pyridyl-type ligand [26], can act as bridging ligand with different structural configurations via the rotation of [–CH₂–CH₂–CH₂–] aliphatic chain between two pyridyl rings as TT, TG, GG, GG' conformation (T = Trans and G = Gauche, shown in Chart 1) to obtain various conformers in polymeric frameworks [27]. Many 1D, 2D, and 3D networks containing transition metal ions and bpp ligands have been reported [26–34]. Terephthalate (BDC²⁻; dianion of terephthalic acid), a rigid dicarboxylate ligand, has been widely used as a bridging ligand with different coordination modes to construct many 2D or 3D MOFs [33–35]. In previous studies, a 3D-entangled or interpenetrating supramolecular networks, by using Zn(II) ion as node and a flexible bpp ligand and a terephthalate ligand as connectors, have been synthesized under hydrothermal conditions [33,34]. The structural characteristics of their 2D or 3D MOFs, built up via the

connectivity of Zn(II) ions with bpp and terephthalate ligands adopting bis-monodentate or bis-bidentate coordination modes (shown in Chart 2), have been studied. However, the relevant water vapor adsorption behavior is interesting and worthy of more study. With our effort on the study of reversible H₂O de-/adsorption behavior during de-/rehydration processes, we report here on the exploration of a 3D polycatenation supramolecular architecture, [Zn(bpp)(BDC)]·1.5H₂O (**1**), which was synthesized by the conventional solution method instead of the hydrothermal method in a previous report [33]. The thermal stability, reversible de-/adsorption of the guest water molecules, and water vapor ad-/desorption isotherms are the focus of this study and investigated by cyclic thermogravimetric analysis (TGA), as well as in situ temperature-resolved X-ray powder diffraction.

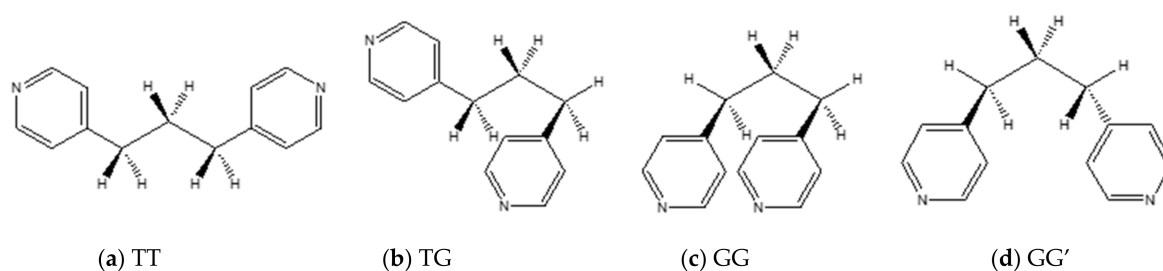


Chart 1. Possible structural configurations of bpp ligand.

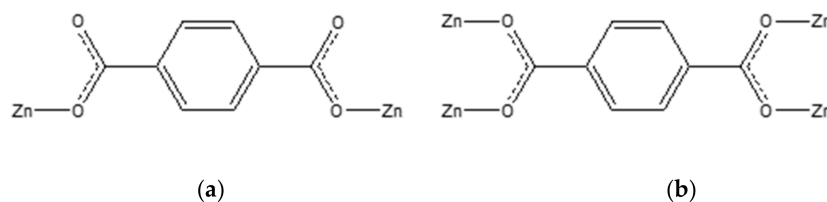


Chart 2. Coordination modes of (a) bis-monodentate and (b) bis-bidentate of BDC²⁻ ligand.

2. Results and Discussion

2.1. Synthesis and Structural Characterization of (**1**)

Different to the hydrothermal synthetic method reported in a previous study [33], compound **1** was synthesized by the conventional solution method with the mixing of Zn(II) salts, bpp, and disodium terephthalate (Na₂BDC) in the H₂O/EtOH solution to obtain colorless, needle-like crystals. The most relevant features of the IR spectrum are those corresponding to the bridging bpp and BDC²⁻ ligands. Absorption bands in the range of 1700–1400 cm⁻¹ can be attributed to the R–CO₂⁻ moiety of the BDC²⁻ ligand and the bpp ligand, with the similar vibrational spectral regions for the two ligands. The IR spectra exhibit a very strong band centered at 1568 cm⁻¹ that can be attributed to vibrational mode representing the mixing stretching motions of C–C and C–N bonds, which is in consistent with the characteristics of the bpp ligand. The broad bands shown in the ranges of 3400–3500 cm⁻¹ indicate the ν(O–H) stretching vibration from H₂O molecules. The reaction yield is obviously increased from 25% synthesized by hydrothermal method [33] to 64% in the present study.

The crystal structure of compound **1**, is redetermined and shows the same crystal system and very close cell parameters as those reported previously [33], with a 3D polycatenation supramolecular architecture being constructed by 2D undulated layered MOFs. The asymmetric unit of compound **1** is composed of a four-coordinated Zn(II) center, one bpp ligand, two halves of two crystallographically independent BDC²⁻ ligands, and one-and-a-half guest water molecules. Each Zn(II) ion is coordinated to two oxygen donors from two BDC²⁻ ligands (Zn–O = 1.957(3) and 2.001(3) Å) and two nitrogen donors from two bpp ligands in TG configuration (Zn–N = 2.046(3) and 2.061(3) Å) in a distorted tetrahedral geometry (Figure 1a). The bond lengths and angles around the Zn(II) ion are listed in Table 1.

In compound **1**, both the BDC²⁻ and TG bpp act as bridging ligands with bis-monodentate coordination mode to form a 2D undulated layered MOF (shown in Figure 1b), which can be viewed as a four-connected net with (4⁴.6²) point symmetry, by using TOPOS [36,37]. The Zn···Zn separations are 10.906 and 10.964 Å for two crystallographically independent BDC²⁻ bridges and 11.955 Å for the bpp bridge, respectively. Interestingly, as shown in Figure 1c, the 3D supramolecular network of compound **1** is constructed by the mutually catenated between 2D undulated layered MOFs. Firstly, adjacent layers are arranged orderly in a parallel manner (green-colored ones in Figure 1d and orange-pink-colored ones in Figure 1e, viewing along the (1,1,0) and (1,−1,0) directions, respectively) and then mutually interlocked with each other to complete its 3D supramolecular architecture (Figure 1c). Intralayers π – π interactions of benzene–pyridyl of BDC²⁻–bpp ligands and pyridyl–pyridyl rings of bpp ligands, which have the ring centroid distances of 4.263 and 3.473 Å, respectively, provide extra stabilization energy on the construction of its 3D network. Relevant interplanar parameters are listed in Table 2. It is also worth noting that the guest water molecules (O(5) and distorted O(6)) intercalated in the vacant spaces are further stabilized by O–H···O hydrogen bonds between the guest H₂O molecules and BDC²⁻ ligands. Related structural parameters for O–H···O hydrogen bonds in **1** are listed in Table 3.

Table 1. Bond lengths (Å) and angles (°) around Zn(II) ion ¹.

Zn(1)–O(3)	1.975(3)	Zn(1)–O(1)	2.001(3)
Zn(1)–N(2) _i	2.046(3)	Zn(1)–N(1)	2.061(3)
O(3)–Zn(1)–O(1)	137.02(1)	O(3)–Zn(1)–N(2) _i	97.62(1)
O(1)–Zn(1)–N(2) _i	110.21(1)	O(3)–Zn(1)–N(1)	106.75(1)
O(1)–Zn(1)–N(1)	97.41(1)	N(2) _i –Zn(1)–N(1)	104.53(1)

¹ Symmetry code: $i = x - 1/2, y - 1/2, z$.

Table 2. Structural parameters of π – π stacking interaction.

R(i) ^a → R(j) ^a	Slip Angle (i,j)/°	Interplanar (i,j) Distance/Å	Horizontal Shift between the (i,j) Ring Centroids/Å	Distance between the (i,j) Ring Centroids/Å
R(1)→R(2)	26.9	3.801	1.930	4.263
R(3)→R(4)	30.2	3.002	1.746	3.473

^a R(1) = C(1)_i–C(2)_i–C(3)_i–C(1)_{ii}–C(2)_{ii}–C(3)_{ii}; R(2) = N(1)–C(9)–C(10)–C(11)–C(12)–C(13); R(3) = N(2)–C(17)–C(18)–C(19)–C(20)–C(21); R(4) = N(2)_{iii}–C(17)_{iii}–C(18)_{iii}–C(19)_{iii}–C(20)_{iii}–C(21)_{iii}. Symmetry codes: $i = x, -y - 1, z - 1/2$; $ii = -x + 1/2, -y + 1/2, -z$; $iii = -x + 1, -y, -z$.

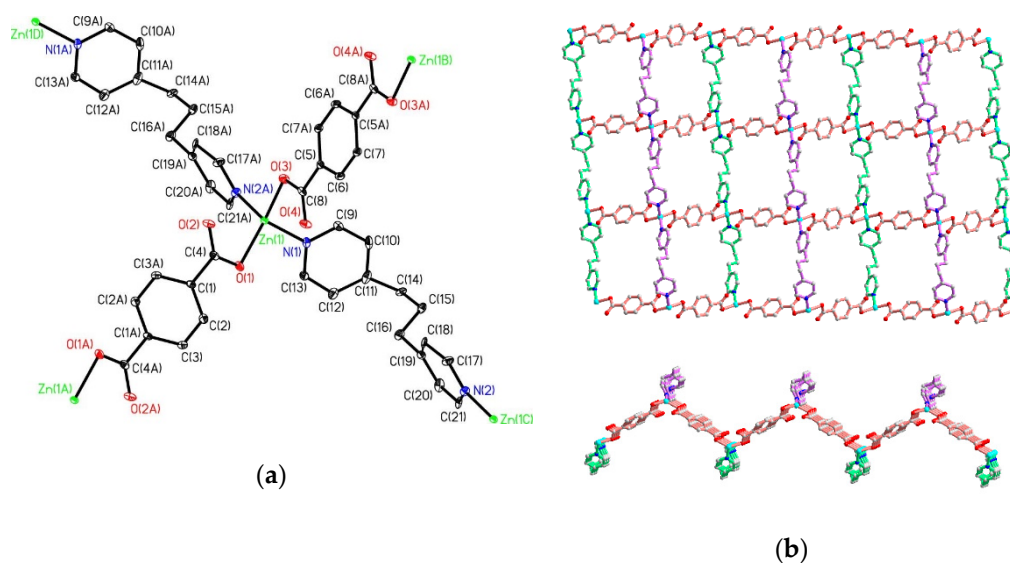


Figure 1. Cont.

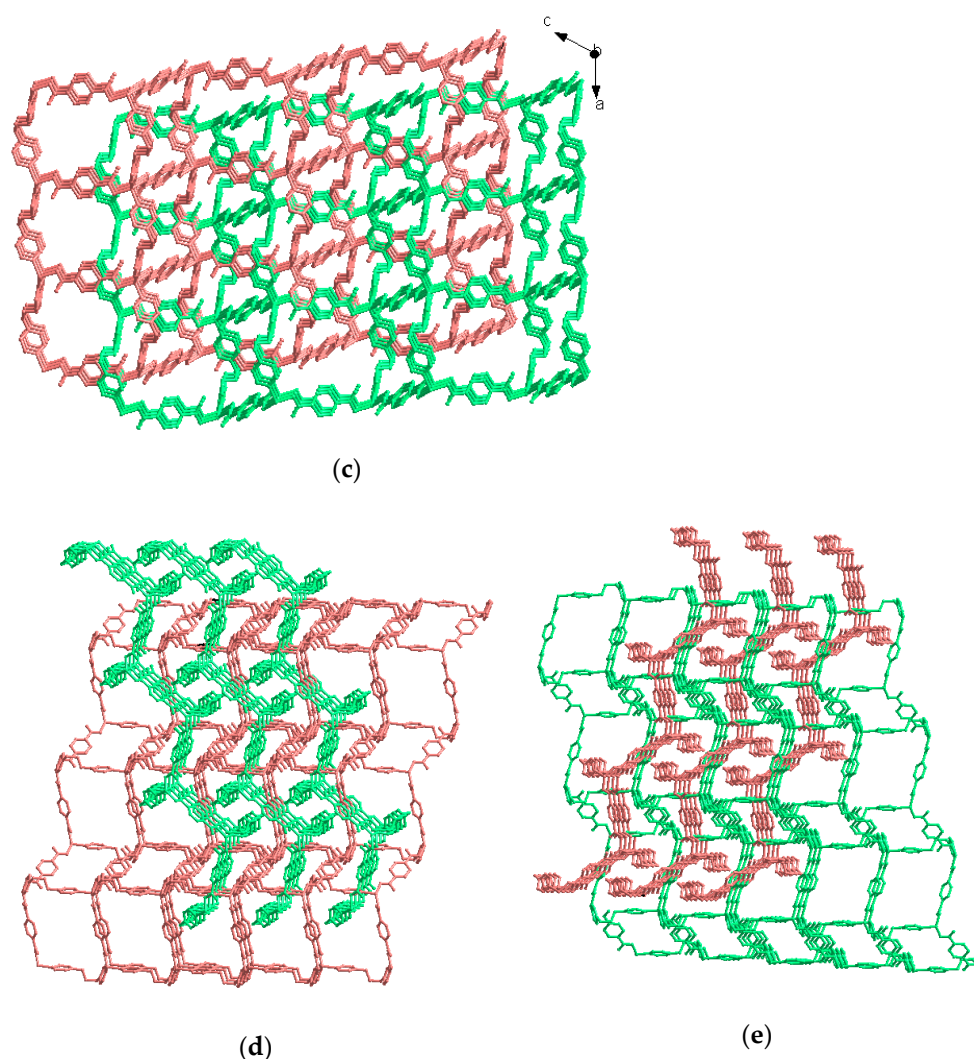


Figure 1. (a) Distorted tetrahedral geometry of Zn(II) ion in compound **1** with atom labeling scheme (30 % thermal ellipsoids); (b) the 2D layered metal–organic framework (MOF) (up) with undulated manner (down); (c) the 3D supramolecular network constructed by the mutually catenated between 2D undulated layered (MOFs); the 3D supramolecular network viewing (d) along the (1,1,0) direction and (e) along the (1,−1,0) direction.

Table 3. Structural parameters of O–H···O hydrogen bonds in compound **1**.

D–H···A	D–H (Å)	H···A (Å)	D···A (Å)	∠ D–H···A (°)
O(5)–H(5A)···O(4)	0.87	2.02	2.862(2)	162
O(5)–H(5B)···O(1) _i	0.84	2.15	2.974(2)	171
O(6)–H(6A)···O(2) _{ii}	0.77	2.13	2.864(2)	161

¹ Symmetry codes: i = x, −y−1, z; ii = −x, −y, −z.

2.2. Thermal Stability of (1)

Thermal stability and thermal-induced structural variation of compound **1** were performed by thermogravimetric analyses (TGA) and in situ temperature-dependent powder XRD measurement, respectively, as shown in Figure 2a,b. The thermogravimetric profile reveals that, during the heating processes in the range of 32.8 to 100.7 °C (shown in Figure 2a), the first weight loss of 6.1% occurred, corresponding to the losses of 1.5 water molecules (calc. 5.9%). The dehydrated species are stable up to 160.1 °C without any weight loss, and then decomposition takes place. The final residue produced at 530 °C is suggested to be ZnO. The structural variations of compound **1** during the thermal dehydration

procedures are further investigated by PRXD (Powder X-ray diffraction) measurements using a high-resolution synchrotron radiation light source to support the results obtained from thermogravimetric analysis. The thermo-stability, as well as phase transitions, of compound **1** were investigated by in situ powder diffraction, as shown in Figure 2b. The powder crystalline structure at 30 °C (red one in Figure 2b) is matching well to its simulation one obtained from single crystal structure (black one in Figure 2b). As temperature increased to 100–150 °C, the desorption process occurred. The crystalline property was retained for a new dehydrated structure. The PXRD measurements are in accordance with the result of thermogravimetric analysis, with compound **1** being thermal stable up to about 200 °C. To verify the de-/adsorption property of one-and-a-half guest water molecules in compound **1**, we have studied the de- and rehydration processes by thermogravimetric measurements under water vapor. It is worth noting that the guest H₂O molecules can be nearly reabsorbed by exposing the samples to water vapor at room temperature. Such heating and cooling procedures were repeated five times to verify the reversibility of de-/adsorption behavior for 1.5 H₂O molecules (Figure 2c).

2.3. Water Sorption Studies of (1)

The cyclic thermogravimetric analyses reveal that compound **1** displays a reversible water de-/adsorption behavior of approximately 1.5 water molecules. Encouraged by the result of cyclic TGA, the gas and water vapor uptake capacities of the dehydrated species were further determined. The crystalline samples **1** were evacuated at 150 °C for 24 h to obtain the activated powder species. The N₂ gas isotherm at 78 K revealed a typical Type-II adsorption profile (Figure 3a) with very low N₂ gas uptake, suggesting only surface adsorption. To explore the water adsorption ability of dehydrated powder species **1**, water vapor sorption isotherms were measured at 298 K. For water vapor adsorption of dehydrated species **1**, the isotherm (Figure 3b) showed a steady increase of adsorbed water vapor at $0 < \text{relative } P/P_0 < 0.89$, with maximum value of $14.65 \text{ cm}^3 \text{ g}^{-1}$ at relative P/P_0 equal to 0.92, nearly equal to 0.60 water molecule being reabsorbed. It is noteworthy that, although the capacity of water sorption was not high, the desorption curve did not follow the adsorption curve but exhibited a significant hysteresis loop with the value of $14.88 \text{ cm}^3 \text{ g}^{-1}$, approximately equal to 0.6 H₂O molecules at lower relative P/P_0 (0.09) value.

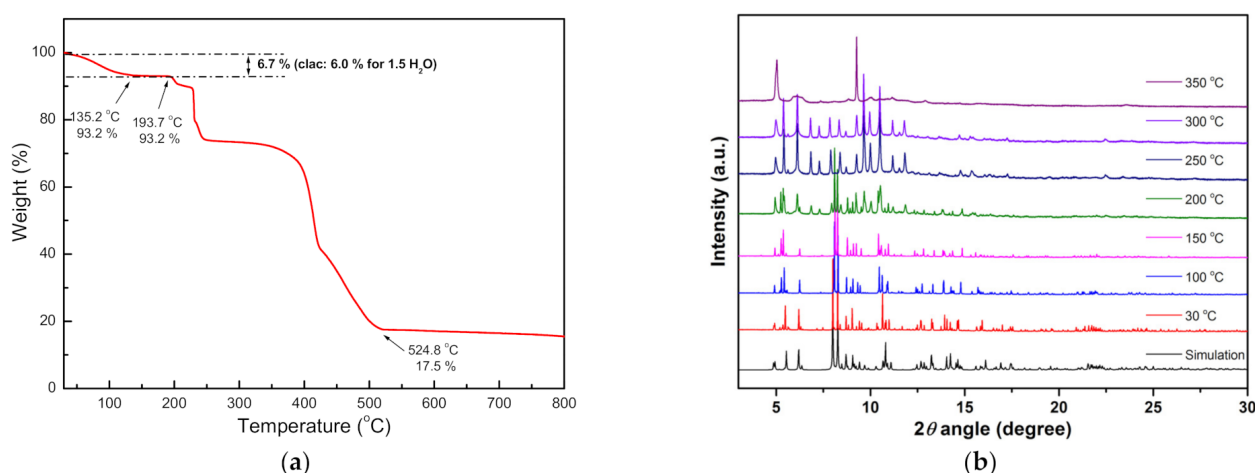


Figure 2. Cont.

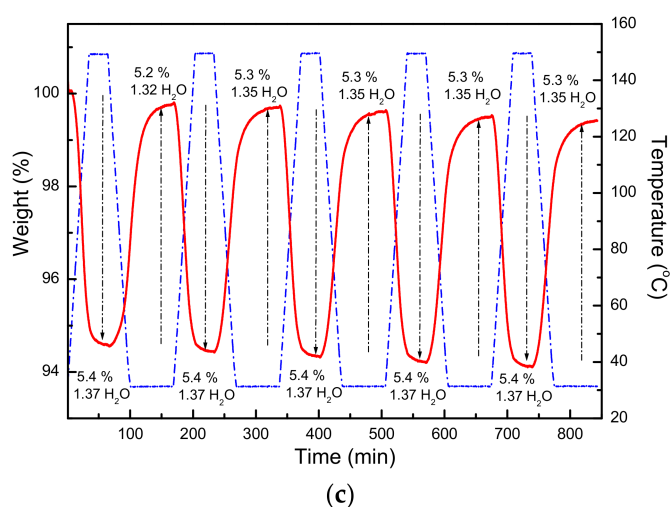


Figure 2. (a) Thermogravimetric analysis of compound 1. (b) Simulation PXRD pattern obtained from single-crystal data and in situ PXRD patterns of compound 1 at selected temperatures. (c) Cyclic thermogravimetric measurements accompanied with the de-/rehydration processes repeated for five times.

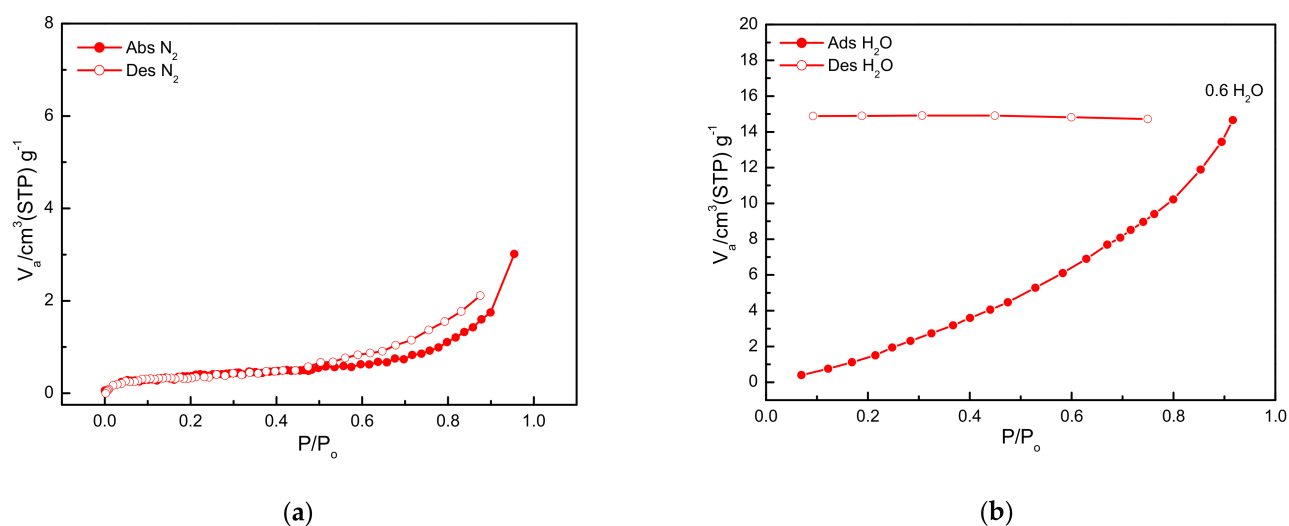


Figure 3. (a) N_2 ad-/desorption isotherms of dehydrated species 1 at 77 K; (b) H_2O ad-/desorption isotherms of dehydrated species 1 at 298 K.

3. Experimental Section

3.1. Materials and Physical Techniques

All chemicals were of reagent grade and used as commercially obtained without further purification. E.A. (C, H and N) were performed using a Perkin-Elmer 2400 (PerkinElmer, Inc. 940 Winter Street Waltham, MA 02451 USA) elemental analyzer, PerkinElmer, Inc. 940 Winter Street Waltham, MA 02451 USA. IR spectra were recorded on a Nicolet FTIR, MAGNA-IR 500 (Thermo Fisher Scientific; Waltham, MA, USA) spectrometer. Thermogravimetric analysis (TGA) was performed on a Perkin-Elmer 7 Series/UNIX TGA7 (PerkinElmer, Inc. 940 Winter Street Waltham, MA 02451 USA) analyzer. The adsorption isotherms of N_2 gas (77 K) and H_2O vapor (298 K) were measured in the gaseous state by using BELSORP-max volumetric adsorption equipment (Microtrac MRB, Nordrhein-Westfalen, Germany). The adsorbate was placed into the sample cell, and then the change of pressure was monitored, and the degree of adsorption was determined by the decrease of pressure at equilibrium state. All operations were computer-controlled automatically.

3.2. Synthesis of $[Zn(bpp)(bdc)] \cdot 1.5(H_2O)$ (**1**)

A water/ethanol (1:1) solution (3 mL) of disodium terephthalate (Na_2BDC) (0.0042 g, 0.02 mmole) was added to a water/ethanol (1:1) solution (6 mL) of ZnF_2 (0.002 g, 0.02 mmole) and 1,3-bis(4-pyridyl)propane (bpp) (0.0079 g, 0.04 mmole) at room temperature (RT). After standing for a few days, colorless, needle-like crystals of compound **1** were obtained with yield of 0.0582 g (64.0%). Anal. Calc. for $C_{21}H_{21}N_2O_{5.50}Zn_1$ (**1**): C 55.46, N 6.16, H 4.65; Found: C 54.98, N 5.93, H 4.55. IR (KBr pellet): $\nu = 3545$ (m), 3468 (m), 1620 (s), 1568 (vs), 1503 (m), 1433 (s), 1403 (s), 1227 (w), 1071 (w), 1031 (m), 823 (m), 746 (m) cm^{-1} .

3.3. Crystallographic Data Collection and Refinements

Single-crystal structural data for compound **1** were collected on a Siemens SMART CCD (Siemens, Germany) diffractometer equipped with graphite monochromated Mo radiation ($\lambda = 0.71073 \text{ \AA}$) at 150 K. Cell parameters were determined using SMART [38] software and refined with SAINT [39] software. Data reduction was performed with the SAINT [39] software and corrected for Lorentz and polarization effects. Empirical absorption corrections were applied with the program SADABS [40]. The structure was solved by direct phase determination, and all nonhydrogen atoms' positions were generated by subsequent difference Fourier map synthesis. All hydrogen atoms were positioned geometrically, except the hydrogen atoms of the water molecules, which were located in the difference Fourier map with the corresponding positions. All calculations were performed by using the SHELXTL-PC V 5.03 software package [41]. Crystallographic data and other pertinent information for compound **1** are summarized in Table 4. The CCDC-2054817 for compound **1** contains the supplementary crystallographic (Supplementary Materials) data for this paper. These data can be obtained free of charge at www.ccdc.cam.ac.uk/conts/retrieving.html (accessed on 29 March 2021).

Table 4. Crystal data and other pertinent information of compound **1**.

Empirical Formula	$C_{21}H_{21}N_2O_{5.50}Zn$	Formula Mass ($g \cdot mol^{-1}$)	454.77
crystal system	Monoclinic	space group	$C2/c$
$a/\text{\AA}$	20.9706(8)	α ($^\circ$)	90
$b/\text{\AA}$	11.4874(5)	β ($^\circ$)	119.0891(11)
$c/\text{\AA}$	19.5792(11)	γ ($^\circ$)	90
$V/\text{\AA}^3$	4121.7(3)	Z	8
D_{calcd} ($g \text{ cm}^{-3}$)	1.466	θ range (deg)	2.381–27.499
μ/mm^{-1}	1.229	Temperature (K)	150(2)
no. of total data collected	13471	no. of unique data	4732
R_1, wR_2^1 ($I > 2\sigma(I)$)	0.0502, 0.1196	R_1, wR_2^1 (all data)	0.0711, 0.1246
GOF ²	1.149	no. of refine params	302

$$^1 R_1 = \sum ||F_o - F_c| | / \sum |F_o|; wR_2(F^2) = [\sum w|F_o^2 - F_c^2|^2 / \sum w(F_o^4)]^{1/2}; ^2 GOF = \{\sum [w|F_o^2 - F_c^2|^2] / (n - p)\}^{1/2}.$$

3.4. In Situ X-ray Powder Diffraction

The powder X-ray diffraction measurements were performed at the 09 A beamline of Taiwan Photon Source (TPS) in National Synchrotron Radiation Research Center (NSRRC). TPS ring was operated at 3 GeV with a typical current 400 mA with top-up injection mode. The 15 keV X-ray source was delivered from an in-vacuum undulator (IU22), and the diffraction patterns were recorded by a position-sensitive detector, MYTHEN 24 K (Dectris, Switzerland). Due to the small gaps between detector modules, two necessary datasets were collected 2° apart and were well calibrated through a NIST standard reference material, LaB_6 (660c). The final data were merged and gridded to give an equal step dataset. The powder sample was sealed in a borosilicate glass capillary (0.3 mm). In situ high temperature experiment was taken by a hot air gas blower with a uniform ramp rate 0.2 degrees/s. The simulated powder diffraction pattern was calculated using the Mercury

program from the Cambridge Crystallographic Data Centre (CCDC), <https://www.ccdc.cam.ac.uk/Community/csd-community/freemercury/> (accessed on 29 March 2021). The simulation setting for X-ray energy and peak shape were 15 keV and 0.03 degree, respectively. The simulated range was from 2 to 50 degree with a constant 0.005-degree interval.

4. Conclusions

In the present work, we successfully described the synthesis, structural characterization, thermal stability and water de-/adsorption behavior of a 3D polycatenation supramolecular network, [Zn(bpp)(BDC)]·1.5H₂O (**1**), which was assembled by a 2D undulated layered MOF via combined parallel and mutually interlocked manners. Interlayers π - π stacking interactions between the bpp and BDC²⁻ ligands and hydrogen bonding interactions between the guest H₂O molecules and BDC²⁻ ligands provided extra energy on the stabilization of the 3D supramolecular architecture. Notably, compound **1** underwent a reversible water de-/adsorption behavior between the dehydrated and rehydrated species during thermal de-/rehydration processes and exhibited significant water hysteresis loop in water vapor ad-/desorption isotherms.

Supplementary Materials: The following are available online at <https://www.mdpi.com/article/10.3390/cryst11040371/s1>, Table S1: Crystal data and structure refinement, Table S2: Atomic coordinates ($\times 10^4$) and equivalent isotropic displacement parameters, Table S3: Bond lengths [Å] and angles [°], Table S4: Anisotropic displacement parameters ($\text{Å}^2 \times 10^3$), Table S5: Hydrogen coordinates ($\times 10^4$) and isotropic displacement parameters ($\text{Å}^2 \times 10^3$).

Author Contributions: C.-C.W. designed the experiments and wrote the paper; W.-C.Y., Z.-L.H. and W.-C.C. performed the experiments, including synthesis, elemental and ligands' identification, structural characterization, thermal-stability measurements and gas and water absorption measurements; G.-H.L. contributed to the single-crystal X-ray data collection and refinement and structural analysis; Y.-C.C. contributed to the powder X-ray diffraction experiments by synchrotron radiation light source and wrote the paper. All authors have read and agreed to the published version of the manuscript.

Funding: This research received no external funding.

Acknowledgments: The authors thank Soochow University, Taipei, and the Ministry of Science and Technology, Taiwan, for financial support.

Conflicts of Interest: The authors declare no conflict of interest.

References

1. Batten, S.R.; Champness, N.R.; Chen, X.M.; Garcia-Martinez, J.; Kitagawa, S.; Öhrström, L.; O'keeffe, M.; Suh, M.P.; Reedijk, J. Terminology of metal-organic frameworks and coordination polymers. *Pure Appl. Chem.* **2013**, *85*, 1715–1724. [[CrossRef](#)]
2. Batten, S.R.; Champness, N.R.; Chen, X.M.; Garcia-Martinez, J.; Kitagawa, S.; Öhrström, L.; O'keeffe, M.; Suh, M.P.; Reedijk, J. Coordination polymers, metal-organic frameworks and the need for terminology guidelines. *CrystEngComm* **2012**, *14*, 3001–3004. [[CrossRef](#)]
3. Griffin, S.L.; Champness, N.R. A periodic table of metal-organic frameworks. *Coord. Chem. Rev.* **2020**, *414*, 213295. [[CrossRef](#)]
4. Natarajan, S.; Mahata, P. Metal-organic framework structures—How closely are they related to classical inorganic structures? *Chem. Soc. Rev.* **2009**, *38*, 2304–2318. [[CrossRef](#)]
5. Blatov, V.A.; O'Keeffe, M.; Proserpio, D.M. Vertex-, face-, point-, Schläfli-, and Delaney-symbols in nets, polyhedra and tilings: Recommended terminology. *CrystEngComm* **2010**, *12*, 44–48. [[CrossRef](#)]
6. Terzopoulou, A.; Nicholas, J.D.; Chen, X.Z.; Nelson, B.J.; Pane, S.; Puigmarti-Luis, J. Metal-organic frameworks in motion. *Chem. Rev.* **2020**, *129*, 11175–11193. [[CrossRef](#)] [[PubMed](#)]
7. Zhu, R.M.; Ding, J.W.; Jin, L.; Pang, H. Interpenetrated structures appeared in supramolecular cages, MOFs, COFs. *Coord. Chem. Rev.* **2019**, *389*, 119–140. [[CrossRef](#)]
8. O'Keeffe, M.; Yaghi, O.M. Deconstructing the crystal structures of metal-organic frameworks and related materials into their underlying nets. *Chem. Rev.* **2011**, *112*, 675–702. [[CrossRef](#)] [[PubMed](#)]
9. Long, J.R.; Yaghi, O.M. The pervasive chemistry of metal-organic frameworks. *Chem. Soc. Rev.* **2009**, *38*, 1213–1214. [[CrossRef](#)]
10. Zhou, H.C.; Long, J.R.; Yaghi, O.M. Introduction to metal-organic frameworks. *Chem. Rev.* **2012**, *112*, 673–674. [[CrossRef](#)]
11. Bentz, K.C.; Cohen, S.M. Supramolecular metallopolymers: From linear materials to infinite networks. *Angew. Chem. Int. Ed.* **2018**, *57*, 14992–15001. [[CrossRef](#)]

12. Karmakar, A.; Paul, A.; Pombeiro, A.J.L. Recent advances on supramolecular isomerism in metal organic frameworks. *CrystEngComm* **2017**, *9*, 4666–4695. [[CrossRef](#)]
13. Alexandrov, E.V.; Blatov, V.A.; Proserpio, D.M. How 2-periodic coordination networks are interweaved: Entanglement isomerism and polymorphism. *CrystEngComm* **2017**, *19*, 1993–2006. [[CrossRef](#)]
14. Wang, X.-L.; Qin, C.; Wang, E.-B.; Li, Y.-G.; Su, Z.-M.; Xu, L.; Carlucci, L. Entangled coordination networks with inherent features of polycatenation, polythreading, and polyknotting. *Angew. Chem. Int. Ed.* **2005**, *44*, 5824–5827. [[CrossRef](#)]
15. Wu, H.; Liu, H.-Y.; Liu, Y.-Y.; Yang, J.; Liu, B.; Ma, J.-F. An unprecedented 2D → 3D metal–organic polyrotaxane framework constructed from cadmium and a flexible star-like ligand. *Chem. Commun.* **2011**, *47*, 1818–1820. [[CrossRef](#)] [[PubMed](#)]
16. Carlucci, L.; Ciani, G.; Proserpio, D.M. Borromean links and other non-conventional links in ‘polycatenated’ coordination polymers: Re-examination of some puzzling networks. *CrystEngComm* **2003**, *5*, 269–279. [[CrossRef](#)]
17. Cui, J.; Alramadan, K.; Li, D.; Lu, J.Y. The first coordination polymer with distinct paired layers. *Inorg. Chem. Commun.* **2013**, *35*, 318–320. [[CrossRef](#)]
18. Abrahams, B.F.; Elliott, R.W.; Hudson, T.A.; Robson, R.; Sutton, A.L. New CuI₂(TCNQ–II) and CuI₂(F₄TCNQ–II) coordination polymers. *Cryst. Growth Des.* **2015**, *15*, 2437–2444. [[CrossRef](#)]
19. Chuang, Y.-C.; Ho, W.-L.; Sheu, C.-F.; Lee, G.-H.; Wang, Y. Crystal engineering from a 1D chain to a 3D coordination polymer accompanied by a dramatic change in magnetic properties. *Chem. Commun.* **2012**, *48*, 10769–10771. [[CrossRef](#)] [[PubMed](#)]
20. Wang, C.-C.; Chung, W.-C.; Lin, H.-W.; Dai, S.-C.; Shiu, J.-S.; Lee, G.-H.; Sheu, H.-S.; Lee, W. Assembly of two Zinc(II)-sulfate coordination polymers with noncovalent and covalent bonds derived from flexible ligands, 1,2-bis(4-pyridyl)ethane (dpe). *CrystEngComm* **2011**, *13*, 2130–2136. [[CrossRef](#)]
21. Zheng, B.; Bai, J. An unprecedented nanoscale trilayered polythreading coordination array hierarchically formed from 2D square grid networks and induced by protonated 1,2-bis(4-pyridyl)ethane. *CrystEngComm* **2009**, *11*, 271–273. [[CrossRef](#)]
22. Mahmoudi, G.; Morsali, A. Novel rare case of 2D + 1D = 2D polycatenation Hg(II) coordination polymer. *CrystEngComm* **2009**, *11*, 50–51. [[CrossRef](#)]
23. Du, M.; Jiang, X.-J.; Zhao, X.-J. Direction of unusual mixed-ligand metal–organic frameworks: A new type of 3-D polythreading involving 1-D and 2-D structural motifs and a 2-fold interpenetrating porous network. *Chem. Commun.* **2005**, *41*, 5521–5523. [[CrossRef](#)]
24. Li, B.L.; Peng, Y.F.; Li, B.Z.; Zhang, Y. Supramolecular isomers in the same crystal: A new type of entanglement involving ribbons of rings and 2D (4,4) networks polycatenated in a 3D architecture. *Chem. Commun.* **2005**, *41*, 2333–2335. [[CrossRef](#)] [[PubMed](#)]
25. Shin, D.M.; Lee, I.S.; Chung, Y.K.; Lah, M.S. Coordination polymers based on square planar Co(II) node and linear spacer: Solvent-dependent pseudo-polymorphism and an unprecedented interpenetrating structure containing both 2D and 3D topological isomers. *Chem. Commun.* **2003**, *39*, 1036–1037. [[CrossRef](#)]
26. Lee, T.-W.; Lau, J.P.-K.; Wong, W.-T. Synthesis and characterization of coordination polymers of Zn(II) with 1,3-bis(4-pyridyl)propane and 4,4′-pyridine ligands. *Polyhedron* **2004**, *23*, 999–1002. [[CrossRef](#)]
27. Wang, C.-C.; Yi, W.-C.; Huang, Z.-L.; Chang, T.-W.; Chien, W.-C.; Tseng, Y.-Y.; Chen, B.-H.; Chuang, Y.-C.; Lee, G.-H. Synthesis, structures, and water adsorption of two coordination polymers constructed by M(II) (M = Ni (1) and Zn (2)) with 1,3-Bis(4-pyridyl)propane (bpp) and 1,2,4,5-benzenetetracarboxylate (BT⁴⁻) ligands. *Polymers* **2020**, *12*, 2222. [[CrossRef](#)] [[PubMed](#)]
28. Li, X.J.; Cao, R.; Bi, W.H.; Wang, Y.Q.; Wang, Y.L.; Li, X. Three interpenetrated frameworks constructed by long flexible N,N′-bipyridyl and dicarboxylate ligands. *Polyhedron* **2005**, *24*, 2955–2962. [[CrossRef](#)]
29. Correa, C.C.; Diniz, R.; Chagas, L.H.; Rodrigues, B.L.; Yoshida, M.I.; Teles, W.M.; Machado, F.C.; de Oliveira, L.F.C. Transition metal complexes with squarate anion and the pyridyl-donor ligand 1,3-bis(4-pyridyl)propane (BPP): Synthesis, crystal structure and spectroscopic investigation. *Polyhedron* **2007**, *26*, 989–995. [[CrossRef](#)]
30. Plater, M.J.; Foreman, M.R.S.; Gelbrich, T.; Hursthouse, M.B. One-dimensional structures of nickel(II) and cobalt(II) coordination complexes {[ML₂(H₂O)₂]-L·H₂O·(ClO₄)₂} (M=Co or Ni; L=1,3-bis(4-pyridyl)propane). *Inorg. Chim. Acta* **2001**, *318*, 171–174. [[CrossRef](#)]
31. Maw-Cherng, S.; Chan, Z.K.; Chen, J.D.; Wang, J.C.; Hung, C.H. Syntheses and structures of three new coordination polymers generated from the flexible 1,3-bis(4-pyridyl)propane ligand and zinc salts. *Polyhedron* **2006**, *25*, 2325–2332.
32. Carlucci, L.; Ciani, G.; Proserpio, D.M.; Rizzato, S. New polymeric networks from the self-assembly of silver(I) salts and the flexible ligand 1,3-bis(4-pyridyl)propane (bpp). A systematic investigation of the effects of the counterions and a survey of the coordination polymers based on bpp. *CrystEngComm* **2002**, *4*, 121–129. [[CrossRef](#)]
33. Chen, S.M.; Zhang, J.; Lu, C.Z. One-pot synthesis of two isomeric zinc complexes with unusual polycatenation motifs. *CrystEngComm* **2007**, *9*, 390–393. [[CrossRef](#)]
34. Wang, G.H.; Li, Z.G.; Jia, H.Q.; Hu, N.H.; Xu, J.W. Topological diversity of coordination polymers containing the rigid terephthalate and a flexible N,N′-type ligand: Interpenetration, polyrotaxane, and polythreading. *Cryst. Growth Design* **2008**, *8*, 1932–1939. [[CrossRef](#)]
35. Erxleben, A. Structures and properties of Zn(II) coordination polymers. *Coord. Chem. Rev.* **2003**, *246*, 203–228. [[CrossRef](#)]
36. Blatov, V.A.; Shevchenko, A.P.; Serezhkin, V.N. TOPOS3.2: A new version of the program package for multipurpose crystal-chemical analysis. *J. Appl. Crystallogr.* **2000**, *33*, 1193. [[CrossRef](#)]

-
37. Blatov, V.A.; Carlucci, L.; Ciani, G.; Proserpio, D.M. Interpenetrating metal–organic and inorganic 3D networks: A computer-aided systematic investigation. Part I. Analysis of the Cambridge structural database. *CrystEngComm* **2004**, *6*, 377–395. [[CrossRef](#)]
 38. *SMART V 4.043 Software for CCD Detector System*; Siemens Analytical Instruments Division: Madison, WI, USA, 1995.
 39. *SAINT V 4.035 Software for CCD Detector System*; Siemens Analytical Instruments Division: Madison, WI, USA, 1995.
 40. Sheldrick, G.M. *Program for the Refinement of Crystal Structures*; University of Göttingen: Göttingen, Germany, 1993.
 41. *SHELXTL 5.03; PC-Version; Program Library for Structure Solution and Molecular Graphics*; Siemens Analytical Instruments Division: Madison, WI, USA, 1995.